Electrochemical Selective Recovery of Heavy Metal Vanadium Oxyanion from Continuously Flowing Aqueous Streams

Author Manuscript

Title: Electrochemical selective recovery of heavy metal vanadium oxyanion from continuously flowing aqueous streams

Authors: T. Alan Hatton, Prof.; Ali Hemmatifar; Nil Ozbek; Cameron Halliday

To be cited as: 10.1002/cssc.202001094

Link to VoR: https://doi.org/10.1002/cssc.202001094

Electrochemical selective recovery of heavy metal vanadium oxyanion from continuously flowing aqueous streams

Ali Hemmatifar, Nil Ozbek, Cameron Halliday, T. Alan Hatton*

Department of Chemical Engineering, Massachusetts Institute of Technology,
77 Massachusetts Avenue, Cambridge, MA 02139, USA

* To whom correspondence should be addressed. E-mail: tahatton@mit.edu

Abstract

An electrochemical flow cell with redox-active electrodes was used for selective removal and recovery of vanadium(V) oxyanions from aqueous streams. The cell relies on intrinsic affinity of the redox-active polymer poly(vinyl)ferrocene (PVFc) and demonstrates selectivity of >10 towards vanadium compared to a background electrolyte in 40-fold abundance. We demonstrate highly selective vanadium removal in the presence of various competing anions (fluoride, bromide, nitrate, and sulfate). Surface elemental analysis reveals significant correlation between PVFc moieties and vanadium-rich regions after adsorption, corroborating the central role of PVFc modulation on vanadium separation. We further propose a vanadium speciation mechanism in which high and low pH environments during adsorption and desorption steps favor formation of, respectively, $H_2VO_3^-$ / HVO_4^{2-} and $H_2VO_3^-$ / H_3VO_4 / VO_2^+. Results have implications for the development and optimization of flow devices, since per our observations, excessively low pH environments during desorption can lead to subsequent re-adsorption of cationic vanadium(V).

Keywords

Electrochemistry, Metallocenes, Vanadium

1. Introduction

Access to clean water is the global and diverse challenge of the 21st century. Continuous discharge of pollutants and wastewater into water sources causes serious health issues and leads to irreversible environmental impacts. Vanadium is a toxic heavy metal, widely used across a multitude of industries—smelting, foundry, textile, ceramic, glass, and refinery to name a few.[1,2] Vanadium can mostly be found in three oxidation states, +3, +4 and +5, with multiple species co-existing across the pH and potential (E_H) landscape.[3] Under most conditions V(V) occurs as vanadate(V) oxyanion ($H_2VO_3^-$/HVO_4^{2-}), while the oxycation of the same oxidation state (VO_2+) can form under highly acidic conditions. V(IV), on the other hand, exists solely as an oxycation (VO^{2+}) stable at low pH and/or under mildly reducing conditions. Finally, various forms of V(III) occur only under strong reducing conditions.[4]

Vanadium species are all toxic, with V(V) being considered as the most toxic form.[5] Vanadium present in the food chain specifically targets respiratory, digestive, metabolic and nervous systems.[6] The International Agency for Research on Cancer (IARC) categorizes vanadium in group 2B—possibly carcinogenic to humans.[7] According to the National Oceanic and Atmospheric Administration (NOAA), the threshold for chronic toxicity effects in freshwater is 19 mg/L and for acute toxicity is 280 mg/L.[8] Interestingly, only a handful of countries have set permissible limits on vanadium in water sources, such as China (50 µg/l in drinking surface water sources)[9] and Italy (140 µg/L for ground water).[10] In addition to the need for vanadium removal from water sources because of its toxic properties, vanadium recovery is highly sought-after due to its applications in steel and iron alloys,[11] as well as in the polymer (as catalyst)[12] and battery industries.[13] Additionally, pure vanadium ores are scarce and generally occur in combination with minerals,[14] making vanadium recovery methods a long-standing

field of study. As such, the presence of naturally-occurring and anthropogenic vanadium in water sources signifies the importance of developments in selective vanadium removal techniques.[15]

The existing methods for removal or recovery of vanadium generally fall into two categories: physiochemical and electrochemical. The most common physiochemical methods include chemical precipitation[10], ion exchange with resins[5,16], membrane filtration, and sorption.[1,17] In the precipitation method, vanadium is precipitated in various forms through the addition of reagents such as ammonium[18] or calcium[19] salts. The sorption methods, while requiring excessive amounts of water, are currently preferable for industrial applications due to their simplicity.[17,20] Various adsorbents have been used for the sorption method such as activated carbon,[21] chitosan films,[22] humic acid,[23] modified ceramic[24] and metal (hydr)oxides.[25] Ion exchange resins are also used for vanadium removal, since vanadium forms anionic species at pH > 3 and cationic species at pH < 2 or 3.[16,26] The main drawback of this method, however, is the requirement for chemical addition during the regeneration process. Likewise, solvent extraction is a fast, high capacity, and selective technique, but the process is complex with high reagent consumption.[27,28] In addition to these physiochemical *removal* methods, various processes exist for *recovery* of vanadium, mostly in the alloy production industry. As an example, some studies suggest the addition of sulfuric or hydrochloric acids for metal dissolution along with a subsequent purification step using techniques such as solvent extraction [29], ion exchange [30] or crystallization [31]. Such methods, again, entail harsh acidic or basic conditions, and require costly and copious amounts of reagents for extraction/precipitation.

Electrochemical methods, and specifically electrosorption processes, are another attractive route for water purification due to their modularity and chemical-free regeneration.

Upon application of a potential difference between electrically-conductive electrodes, charged ions are removed from the feed water and electrostatically held within their respective electrodes. In general, the capacity of this process depends mainly on (1) electrical double layer capacity, which is affected by ion solution concentration and applied voltage and (2) pseudocapacity due to faradaic reactions, which depends on functional groups on the electrode surface and chemical characteristics of the solute.[32] Functionalizing the electrode surfaces with different active materials can potentially enhance the removal selectivity for ions of interest.[33–37] As an example, metallopolymer-based electrodes such as poly(vinyl)ferrocene (PVFc) have high selectivity and ion-uptake capacity for heavy metal oxyanions such as chromium and arsenic. This is due to electrochemically activated chemical interactions and inherently more polarizable electron clouds of heavy metal oxyanions compared to the competing anions, which result in greater charge transfer, stronger binding, and therefore selectivity towards these species.[38] Despite their promise, however, continuous-flow electrosorption systems with selectivity for heavy metals have rarely been pursued in the literature. In fact, to the best of our knowledge, there are no studies on vanadium-selective continuous-flow recovery methods via electrosorption. The closest study is perhaps the work of Brennsteiner et al.,[39] where they employed electrosorption of heavy metals (such as cadmium, lead, copper and nickel) in a non-selective manner using a flow-through electrochemical cell with non-functionalized carbon-based electrodes followed by a desorption step at various potentials.

In this work, as shown in **Figure 1**, we develop a continuous-flow system for electrosorptive removal and recovery of V(V) oxyanions from aqueous solutions using redox-active electrodes. To this end, we employ an intrinsic affinity of redox-active ferrocene moieties (in the form of PVFc) towards metal oxyanions[38,40] and fabricate an asymmetric flow cell for

selective vanadium removal. The redox-active anode and cathode used are, respectively, PVFc-functionalized carbon nanotubes (CNTs) and conducting polymer polypyrrole (PPy) doped with anionic surfactant sodium dodecylbenzenesulfonate (SDBS). Schematics of electrode redox reactions are given in **Figures 1(c)** and **1(d)**. PVFc-CNT anode oxidation during the adsorption step results in selective sequestration of vanadates, while simultaneous reduction of the PPy-DBS cathode contributes to cation adsorption. During the desorption, the reverse redox reactions result in expulsion of adsorbed ions. We perform detailed adsorption studies under both batch and flow conditions and demonstrate vanadium removal selectivity of >10 over a background anion in 40-fold abundance in the presence of competing anions. Our study also incorporates observations from various analytical methods and proposes a detailed mechanism for vanadium speciation during continuous-flow adsorption/desorption based on the flowrate and local pH environments.

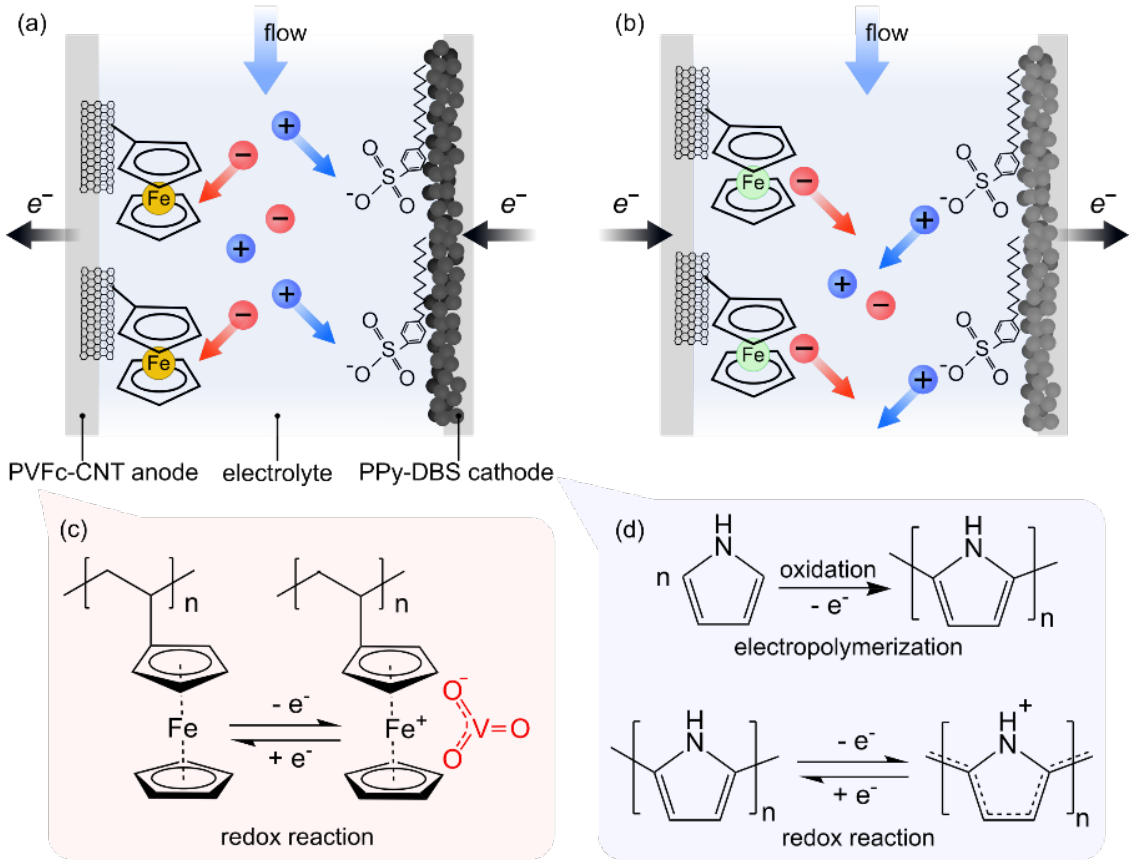

Figure 1. Schematic of the asymmetric redox flow cell with PVFc-CNT anode and PPy-DBS cathode during ion adsorption and desorption steps. (a) PVFc-functionalized CNT anode oxidation during the adsorption step results in selective sequestration of anionic species, while simultaneous reduction of DBS-doped PPy cathode contributes to the cation adsorption. (b) Subsequent reduction of PVFc-CNT and oxidation of PPY-DBS expels the adsorbed ions, forming a brine stream. (c) Electrochemical redox reaction of PVFc, and (d) electropolymerization and redox reaction of PPy.

2. Materials and methods

2.1. Materials

Poly(vinyl)ferrocene (PVFc) obtained from Polysciences, Inc. was used as received. Multi-walled carbon nanotubes (CNTs, OD 6-13 nm, L 2.5-20 μm), pyrrole monomer, and sodium dodecylbenzenesulfonate (SDBS) anionic surfactant were obtained from Sigma Aldrich. The

conductive substrates used in preparation of both anode and cathode electrodes was AvCarb 1071 HCB carbon cloth (Fuel Cell Earth LLC, USA).

2.2. Electrode preparation

PVFc-CNT electrodes were prepared via drop-casting of specific volumes of PVFc-CNT dispersion (in chloroform) on carbon cloth substrates as described elsewhere[38,41]. The dispersion was prepared as follows. A solution of 80 mg PVFc and 40 mg multi-walled CNT dispersed in 10 ml chloroform was mixed with a second solution of 40 mg CNT in 10 ml chloroform, resulting in a stock solution of PVFc-functionalized CNT with 4 mg ml^{-1} PVFc loading. Stock solutions before and after mixing were sonicated in an ice bath for at least 1 h to ensure uniform dispersion and stored in a fridge at 4° C. The resulting dispersion was drop-cast on carbon cloth substrates of 2x2, 2x4, or 2x12 cm size with PVFc loading varying between 0.2 and 0.8 mg cm^{-2} (equivalent to 50 and 200 µl cm^{-2}) and dried under atmosphere for 10 min. Refer to **Results and Discussions** section for more details.

PPy-DBS electrodes were prepared through electropolymerization of pyrrole monomer in the presence of SDBS anionic surfactant (as described by Ren et al.[42]) onto carbon cloth substrates. The electrolyte was an aqueous solution of 0.3 M pyrrole monomer and 0.1 M SDBS. The electropolymerization of DBS-doped PPy was performed using a VersaStat4 potentiostat (Princeton Applied Research, USA) with a two-electrode configuration under a constant current density of 1 mA cm^{-2} and a titanium sheet counter electrode (McMaster Carr, USA). A custom-built electrodeposition cell capable of uniform deposition on substrates up to 4x14 cm size was used.

2.3. Electrochemical characterization

Electrochemical characterization, namely, cyclic voltammetry (CV), batch adsorption and flow cell experiments, as well as PPy electropolymerization were performed on a VersaSTAT4 potentiostat (Princeton Applied Research, USA). CV and batch adsorptions were conducted using a three-electrode configuration with a Ag/AgCl reference electrode (BASi, USA), while PPy electropolymerization and flow cell adsorption/desorption cycling used a two-electrode configuration setup.

2.4. Electrochemical flow system

The experimental setup consisted of our custom-made, axial-flow electrochemical cell, a 1 L solution reservoir, a peristaltic pump (Cole-Parmer, USA), a four-way inlet valve, a miniature flow-through conductivity sensor (ET916, eDAQ Pty Ltd., Australia), and an automated fraction collector (Model 2128, Bio-Rad, USA) for effluent solution fractionation. Refer to **Figure 2** for an image of the experimental setup and three-dimensional drawing of the electrochemical cell.

The electrochemical cell consisted of a 2x12 cm carbon cloth electrode pair separated by a glass microfiber filter (Thermo Fisher Scientific, USA) and sandwiched between a pair of graphite current collectors (See **Figure 2b**). The cell stack was then placed between a pair of polypropylene end-plates and sealed with a 100 μm thick silicon rubber gasket, O-rings, and fasteners. An inlet and an outlet port were incorporated into the end-plates for water delivery to, and collection from, the cell. We estimate the cell volume to be ~3.9 ml by gravimetric measurement of the cell under dry and wet conditions.

We performed flow-cell vanadium oxyanion removal experiments in the presence of various competing anions and quantified their removal selectivity with respect to the background electrolyte anion (20 mM $NaClO_4$ in all cases), as described in the following. To

evaluate vanadium selectivity with respect to the background anion, a feed solution containing 0.5 mM KVO_3 and 20 mM $NaClO_4$ (a 40x mixing ratio) was used. Selectivity for vanadium with respect to ClO_4^- was also compared to selectivity toward multiple competing anions (against ClO_4^-) using a feed solution with 20 mM $NaClO_4$ and 0.5 mM concentration of VO_3^-, Br^-, NO_3^-, and SO_4^{2-} (0.5 mM each). In order to reduce dissolved oxygen levels, each solution was purged with pure N_2 prior to all experiments.

The adsorption and desorption steps were performed potentiostatically, respectively at 1.1 V and -0.5 V, under open-loop and single-pass flow with continuous 0.48 ml min^{-1} flowrate. Charging at 1.1 V ensures full oxidation of PVFc and reduction of PPy-DBS polymers, while limiting the parasitic reactions such as substrate (carbon cloth) oxidation and dissolved oxygen reduction. Similarly, discharging at -0.5 V ensures full reduction of PVFc and oxidation of PPy-DBS electrodes. Prior to the adsorption step, the cell was flushed with DI water for at least 15 min. The influent solution was then switched to the vanadium-containing stream and a voltage of 1.1 V was immediately applied to the cell. A voltage of -0.5 V was subsequently applied during desorption to regenerate the cell.

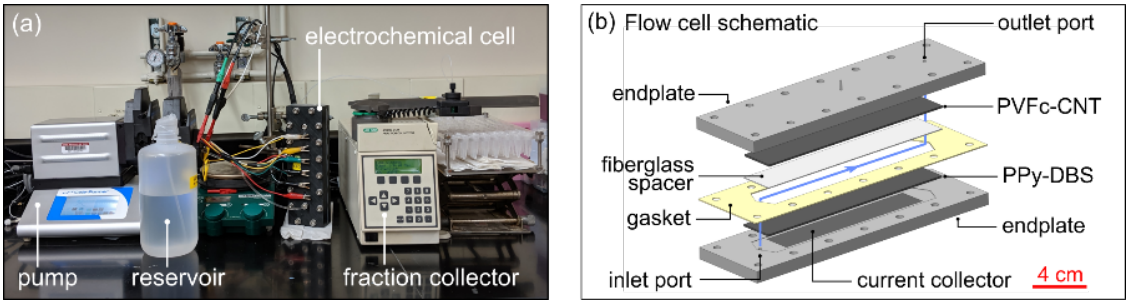

Figure 2. (a) Image of the continuous-flow system consisting of our electrochemical cell, an influent reservoir, a peristaltic pump, an automated fraction collector, and a flow-through conductivity sensor (not shown). (b) Three-dimensional drawing of the electrochemical cell with a pair of 2x12 cm electrodes, fiberglass spacer, current collectors, and a gasket sandwiched between a pair of polypropylene end-plates.

196

197

198 **2.5. Active material surface characterization**

199 The electrode surfaces were surveyed by scanning electron microscopy (SEM) and energy
200 dispersive X-ray spectroscopy (EDX) via a Zeiss Merlin High-Resolution instrument. The
201 characterizations were performed to study the surface morphology and elemental composition
202 of electrode surfaces during electrochemical modulation. SEM analysis was done with a 15
203 keV beam energy, 0.5 nA beam current, and 10 mm working distance in a high-vacuum
204 chamber. EDX elemental analysis and mapping were analyzed with APEX software (AMETEK
205 Inc., USA).

206

207 **2.6. Elemental quantification of vanadium**

208 The concentration of elemental vanadium was quantified spectroscopically via inductively
209 coupled plasma optical emission spectrometry (ICP-OES, Perkin Elmer, Optima 8000) at
210 290.88 nm wavelength. A 2% w/w HNO_3 solution was prepared from 70% HNO_3 (Sigma
211 Aldrich, USA) and was used as blank samples and for dilution of solutions when necessary.
212 Calibration standards were prepared from vanadium stock solution (1000 ± 2 mg L^{-1}, 2% w/w
213 HNO_3, Fluka Analytical TraceCert, USA) by serial dilution using the prepared blank solution. A
214 linear curve fit was performed with four standards (0.1, 0.5, 1 and 2 mg L^{-1} V) with regression
215 coefficient (R^2) of 0.999. An example of the calibration curve and the vanadium emission
216 spectrum is shown in **Figure S1** of **Supplementary Information** (SI). Samples from batch and
217 flow experiments were diluted either 10x or 20x to a total volume of 2 ml prior to quantification
218 and were measured in triplicate to yield an average reading. The limit of detection (LOD) and
219 quantification (LOQ) were estimated to be 2.2 and 7.6 ppb V (or 0.044 and 0.145 μM),

respectively. LOD and LOQ were obtained from 10 repetitive readings of the blank solution (2% w/w HNO_3) and calculated as $3\sigma/s$ and $10\sigma/s$, with σ and s being standard deviation of the readings and slope of the calibration curve, respectively.

2.7. Quantification of competing anions

The content of competing anions—including fluoride (F^-), bromide (Br^-), nitrate (NO_3^-), sulfate (SO_4^{2-}), and perchlorate (ClO_4^-)—was quantified using ion-exchange chromatography (IC) on a Dionex ICS-1600 (Thermo Scientific, USA) equipped with a Dionex IonPac AS22 column and Dionex AERS 500 carbonate suppressor. The quantification was carried out using an isocratic carbonate/bicarbonate eluent (4.5 mM Na_2CO_3 and 1.4 mM $NaHCO_3$), with 0.7 ml min^{-1} flowrate and 15 min sample run-time. Aliquots from multi-component batch and flow experiments were diluted respectively 10x and 2x (from aliquots of 150 µl and 500 µl, respectively) and loaded into 0.5 ml capped vials for quantification. A set of independent IC measurements each for an individual anion was performed for the purpose of (1) standard calibration calculations and (2) confirmation of anion presence in the multi-component samples via retention time matching. A comparison of chromatograms for standard solutions and multi-component samples is shown in **Figure S2** of **SI**.

3. Results and discussions

3.1. Surface morphology and capacity matching

Figure 3 shows high resolution SEM micrographs of the pristine carbon cloth (left panels), PPy-DBS cathode (middle panels), and PVFc-CNT anode (right panels) at three magnification levels (top to bottom). **Figures 3(d)-(f)** correspond to a 2x2 cm PPy-DBS electrode with 375 mC cm^{-2} charge density electrodeposited at 1 mA cm^{-2} current density. Under these conditions, PPy forms a uniform coating with roughly 50-80 nm thickness on the surface of the CC substrate

(see **Figures 3(e)** and **3(f)**). Such a thin polymer coating and therefore short diffusion pathway is particularly beneficial for cation insertion and expulsion into and from the film, as the redox kinetics in PPy-DBS are strongly governed by diffusive transport of cations and background anions.[43–45] On the other hand, PVFc-functionalized CNT fibers in **Figures 3(g)-(i)** (immobilized by drop-casting a 200 µl dispersion solution onto 2x2 cm substrate or 0.2 mg_{PVFc} cm^{-2}) form nanoporous bundles with high surface area morphology on the anode substrate. The PVFc metallocene sites immobilized on the surfaces of CNTs are thus highly accessible to the counterions, which enables the anode to readily capture and release counterions upon electrochemical modulation.

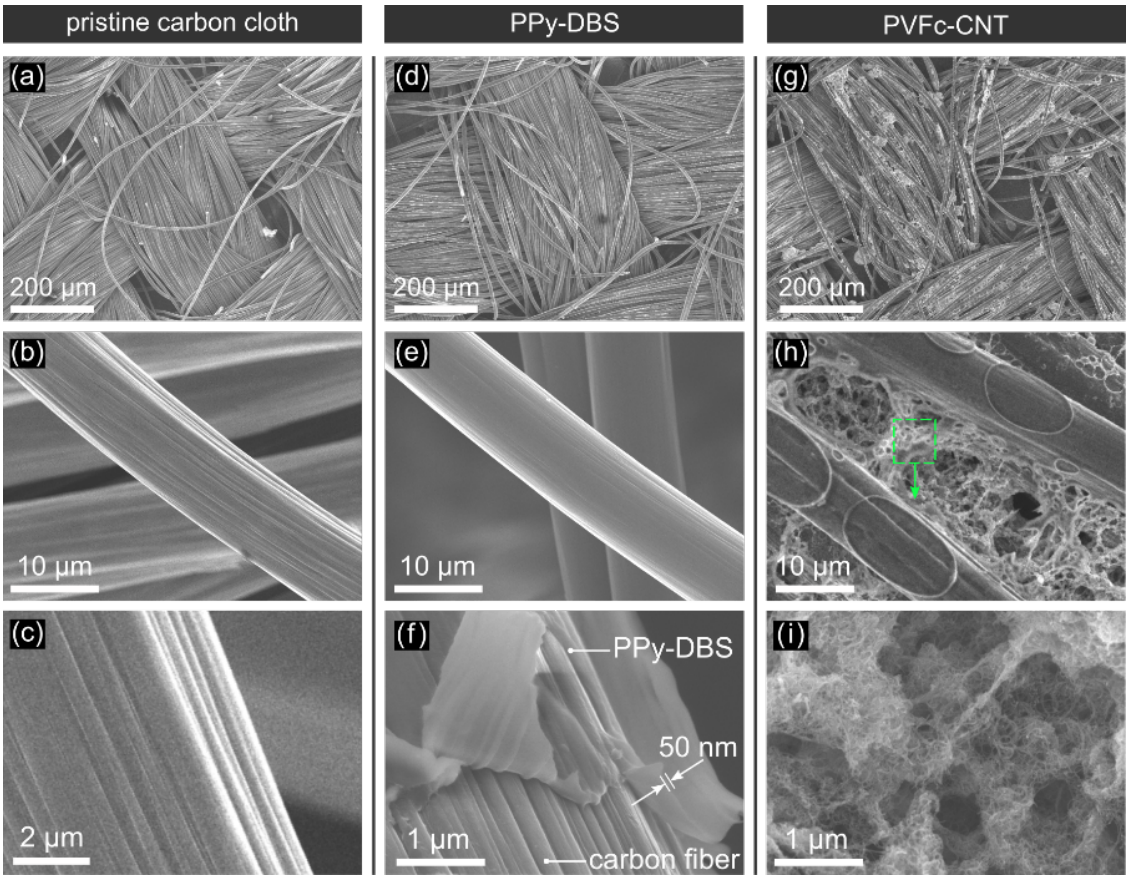

Figure 3. EM micrographs of pristine carbon cloth substrate (left panels), PPy-DBS cathode with 375 mC cm^{-2} surface charge density (middle panels), and PVF-CNT anode with 0.2 mg

cm^{-2} PVFc loading (right panels), with increasing magnification (top to bottom panels). The electrodeposited conductive polymer PPy is seen to form uniform coating of 50-80 nm thickness on carbon fibers, while PVFc-functionalized CNTs form bundles with nanoporous morphology. Extremely thin PPy-DBS and highly porous PVF-CNT respectively enhance cation insertion/expulsion and anion transport upon electrochemical modulation.

The morphological dissimilarity of the anode and cathode eludes to the importance of capacity matching of our PVFc-CNT/PPy-DBS asymmetric system. In fact, optimal capacity matching of the electrodes plays a central role in the performance of asymmetric electrochemically-modulated systems, as it improves the overall cell efficiency and capacity utilization by avoiding surface parasitic reactions.[46,47] To this end, we conducted a series of cyclic voltammetry experiments with the three-electrode configuration on asymmetric cells with various PPy loadings (and a fixed PVFc loading) and calculated the capacity of the individual electrodes (**Figure 4**). The aim here is to determine the optimum ratio between the PVFc and PPy loadings. Specifically, seven identical PVFc-CNT anodes each with 0.2 mg cm^{-2} PVFc loading as well as seven PPy-DBS cathodes with charge density ranging between 50 to 1250 mC cm^{-2} were prepared on 2x2 cm substrates. CV's of electrode pairs against a Ag/AgCl reference (BASi, USA) were then performed individually on anodes (-0.2 V to +0.8 V) and cathodes (-1 V to 0 V) in 0.1 M $NaClO_4$ electrolyte at 5 mV s^{-1} scan rate. **Figure 4(a)** demonstrates the resulting voltammograms for selected electrode pairs with 50, 375, and 750 mC cm^{-2} PPy-DBS cathodes and shows stable and reversible redox activity on both electrodes. The specific capacitance of the individual electrodes was calculated as

$$C = \frac{1}{2m_{\mathrm{PVFc}}\, v}\frac{\oint I\, \mathrm{d}V}{\Delta V} \qquad (1)$$

with m_{PVFc}, I, V, ΔV and v being PVFc loading mass (0.8 mg), measured current, applied potential, and CV potential window (1 V) and scan rate (5 mV s^{-1}), respectively. Note, we here use PVFc mass to normalize the capacity of both anode and cathode, since normalization by individual electrode active material tends to obscure the *capacity* values and the capacity matching process. As evident from **Figure 4**, the CV of PPy-DBS electrode is a strong function of PPy loading, while PVFc-CNT voltammograms appear to be of the same size and shape at various PPy loadings. **Figure 4(b)** quantifies this dependency and shows constant and linearly-increasing capacitance for PVFc-CNT and PPy-DBS electrodes, respectively. Intersection of the two graphs at around 375 mC cm^{-2} confirms the capacity matching between 0.2 mg cm^{-2} PVFc-CNT anode and 375 mC cm^{-2} PPy-DBS cathode. These values thus serve as a baseline for fabrication and scaling of our asymmetric electrochemical cell for both batch and flow cell vanadium recovery efforts discussed in the following.

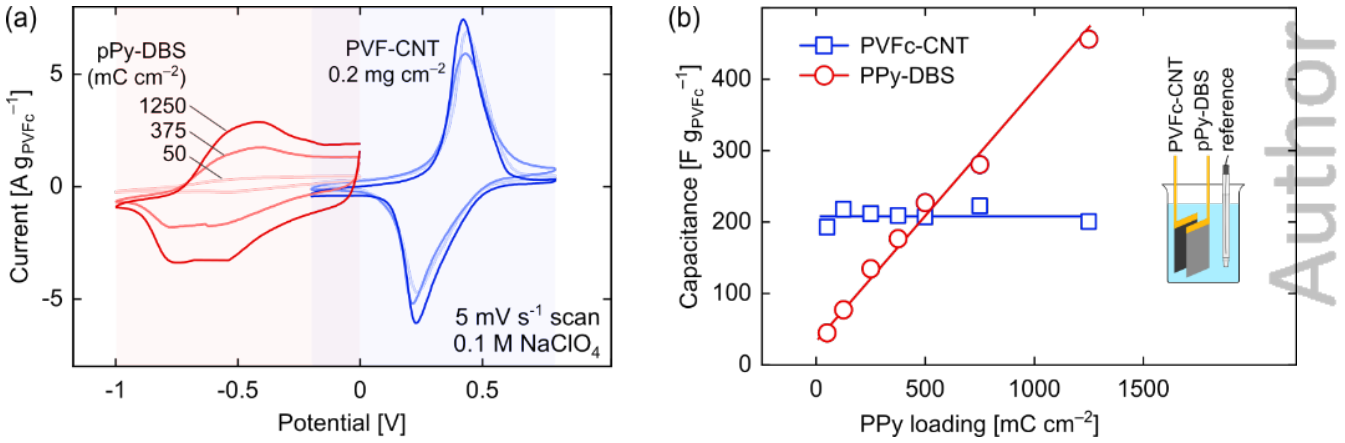

Figure 4. Capacity matching of a PVFc-CNT/PPy-DBS asymmetric system by a series of CVs on cells with 0.2 mg cm^{-2} PVFc loading and various deposited amounts of PPy in the range of 50 to 1250 mC cm^{-2}. (a) Selected anode and cathode CVs on cells with 50, 375, and 1250 mC cm^{-2} PPy loading. (b) Calculated capacitance of each electrode (per PVFc mass) versus deposited PPy amount shows roughly constant and linearly increasing anode and cathode capacitance, respectively. Intersection of the two lines indicates capacity matching between

0.2 mg cm^{-2} PVFc-CNT and 375 mC cm^{-2} PPy-DBS. All CVs were performed in 0.1 M $NaClO_4$ electrolyte at 5 mV s^{-1} scan rate.

3.2. Selective vanadium recovery in batch system

Anion selectivity and vanadium adsorption kinetics

We used the capacity matching results discussed in **Section 3.1** as the baseline and prepared an electrochemical cell with 0.8 mg cm^{-2} PVFc and 1.5 C cm^{-2} PPy loading on 2x4 cm CC substrates. This scaled-up cell was used to study the adsorption kinetics and relative selectivity of vanadium (vs. ClO_4^- background anion) in the presence of common competing anions. The electrolyte used was 20 mM $NaClO_4$ with KVO_3, NaF, NaBr, $NaNO_3$, and Na_2SO_4 competing salts (1 mM each) with a total volume of 7 ml. To ensure near-complete depletion of V, we intentionally used a PVFc loading in excess with a total of 30 µmoles Fc centers compared to 7 µmoles KVO_3. We quantified the selectivity for each anion (vanadate and competing anions) present in the solution by operating our cell at a constant potential of +0.8 V PVFc-CNT (vs. Ag/AgCl) and measuring the anion content in 1 h intervals. +0.8 V operation voltage, as per our previous CV observations, is sufficiently higher than the PVFc activation potential and ensures complete PVFc oxidation. **Figure 5** summarizes the absorption results for our cell operated for >6 h. The inset of **Figure 5(a)** shows the concentration profile of individual anions in the first 3 h of adsorption at +0.8 V. Interestingly, the results show ~25-fold reduction in vanadium concentration (from 1 mM down to 40 µM), while exhibiting insignificant adsorption of F^-, Br^-, NO_3^-, and SO_4^{2-}. This clear difference in adsorption of V versus the competing anions translates into a high level of vanadium selectivity. We calculate selectivity of anion i against the background as

$$S_i = \frac{(\Delta c/c_0)_i}{(\Delta c/c_0)_{\mathrm{ClO_4^-}}}, \quad (2)$$

where c_0 is the initial concentration (1 mM here) and Δc is the concentration change after a given time. **Figure 5(a)** demonstrates selectivity of our batch system for various anions at $t = 3\ \mathrm{h}$ and shows vanadium selectivity of >10, significantly higher than that of Br^- (~2.4), F^- (~1.7), NO_3^- (~0.6) and SO_4^{2-} (~0).

The aforementioned experiment at +0.8 V was complemented by a separate control experiment under open-circuit operation to study the adsorption kinetics of vanadates. As evident in **Figure 5(b)**, the open-circuit experiment did not yield any noticeable uptake of vanadium by the electrodes, confirming the central role of PVFc redox modulation on vanadium electrochemical separation. Note that as per the inset of **Figure 5(b)**, total V concentration plateaus at 40 μM after ~3 h of adsorption owing to competition for the adsorption sites by the perchlorate ion, which is in significant excess but has a much lower binding strength, resulting in a large separation factor between vanadium and ClO_4^- of ~500x after 3 h adsorption. The V adsorption progression in **Figure 5(b)** can be described successfully by a first order kinetics model $q/q_e = 1 - e^{-k_1 t}$, where q_e and q are the adsorbed amounts at equilibrium and time t, respectively, and k_1 is the adsorption rate constant ($q_e = 53.6\ \mathrm{mg\ g_{PVFc}^{-1}}$ and $k_1 = 1.11\ \mathrm{h^{-1}}$). As expected, the PVFc utilization ratio (molar ratio of adsorbed V to PVFc loading on the right axis of **Figure 5(b)**) shows an equilibrium value of about 22% due to excess PVFc loading and subsequent complete depletion of V. Lower active material loading, however, leads to a higher utilization ratio. **Figure S3** of the **SI** shows our separate batch adsorption under the same conditions but with 8x smaller electrodes of 1x1 cm size (equivalent to 3.75 μmoles PVFc), which resulted in higher utilization ratio of around 50% (equivalent to 120 $\mathrm{mg\ g_{PVFc}^{-1}}$) in less than 2 h adsorption time.

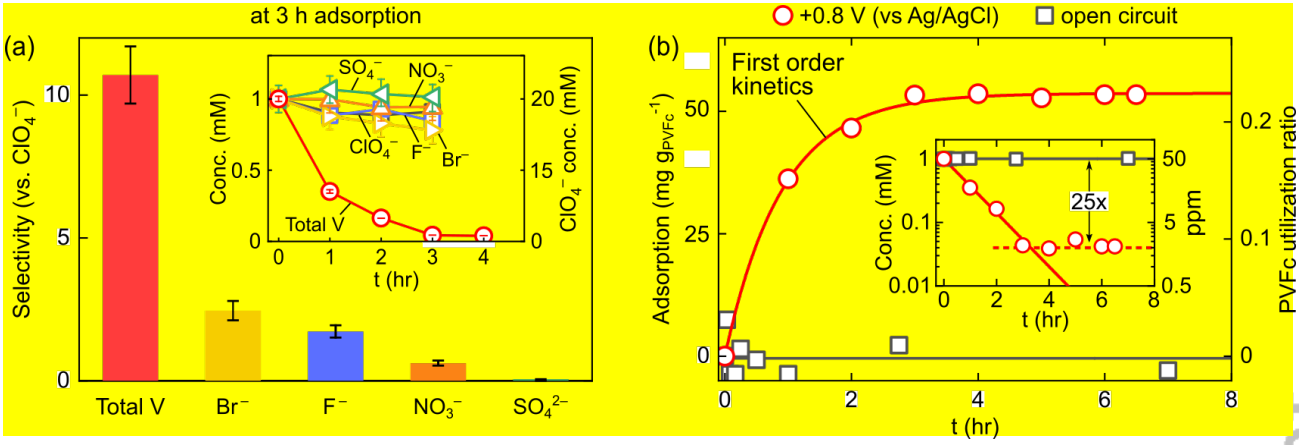

Figure 5. Selective electrochemical removal of vanadate from aqueous solutions in presence of common competing anions using PVFc-CNT/PPy-DBS and a Ag/AgCl reference in batch operation. (a) Calculated selectivity of individual anions (0.5 mM each) with respect to background anion (20 mM) after 3 h adsorption at +0.8 V PVFc-CNT (vs. Ag/AgCl) shows >10 selectivity for vanadium and <2.5 for competing anions. Inset shows near-complete removal of vanadium after 3 h adsorption. (b) Adsorption kinetics for operation at +0.8 V and under open circuit conditions. The former closely follows the first order kinetics model $q/q_e = 1 - e^{-k_1 t}$ and shows a 25-fold vanadium concentration reduction (see the inset). Operation under open circuit conditions for a duration of 6 h does not show any appreciable vanadium removal.

Vanadium elemental mapping and localized adsorption

We confirmed that the adsorption of vanadium is indeed achieved by the redox-active metallocene polymer PVFc by performing a set of batch adsorption experiments and conducting a survey of the elemental presence of vanadium on the electrode surfaces via X-ray microanalysis. To this end, we conducted an adsorption test at +0.8 V PVFc-CNT (vs. Ag/AgCl) for a duration of 2 h. A separate control experiment under the same conditions but at open-circuit was performed as well. The electrolyte used in both experiments was 20 mM $NaClO_3$ and 1 mM KVO_3. The results are reflected in **Figure 6**, in which we present SEM

368 micrographs with superimposed elemental maps (left panels) as well as EDX spectra of the
369 corresponding regions (right panels) for both anode and cathode at the end of 2 h experiments
370 elaborated above. Elemental maps in the control experiment at open-circuit confirm the
371 presence of iron clusters color-coded as red on the PVFc-CNT anode (note iron Kα and Kβ
372 characteristic peaks in panel (b)), while clearly showing no V adsorption on either electrode
373 (color-coded as green in panels (a)-(b) and (e)-(f)). On the other hand, PVFc charging at +0.8
374 V (vs. Ag/AgCl) resulted in localized adsorption of V primarily at the iron centers of PVFc-
375 functionalized CNTs as evident from color-coded EDX map of **Figure 6(c)**. Note also the
376 corresponding Kα and Kβ emission lines in **Figure 6(d)**. While PVFc-CNT demonstrated
377 significant V adsorption, the EDX elemental map and spectrum of PPy-DBS after +0.8 V
378 adsorption do not show any V uptake during the 2 h adsorption process (see **Figure 6(g)** and
379 **6(h)**).

380 We interpret these observations as strong evidence that V adsorption is achieved
381 specifically by interaction with the ferrocene sites of the PVFc polymer, in accordance with a
382 previous report on electrochemical capture of Cr and As oxyanions by PVFc [38]. As a side note,
383 on comparing the energy spectra of **Figures 6(b)** and **6(d)**, we observe an increase in peak
384 height ratio of Cl to Fe (from 0.26:1 to 0.87:1) on the PVFc-CNT anode after adsorption at +0.8
385 V, verifying concurrent perchlorate adsorption on the electrode. To summarize, our results
386 show localized V adsorption onto PVFc-functionalized CNTs, corroborating the central role of
387 redox-modulation of PVFc in selective V uptake with no contribution from the PPy-DBS
388 electrode other than counter ion adsorption, which ensures electrical neutrality in the bulk
389 solution.
390

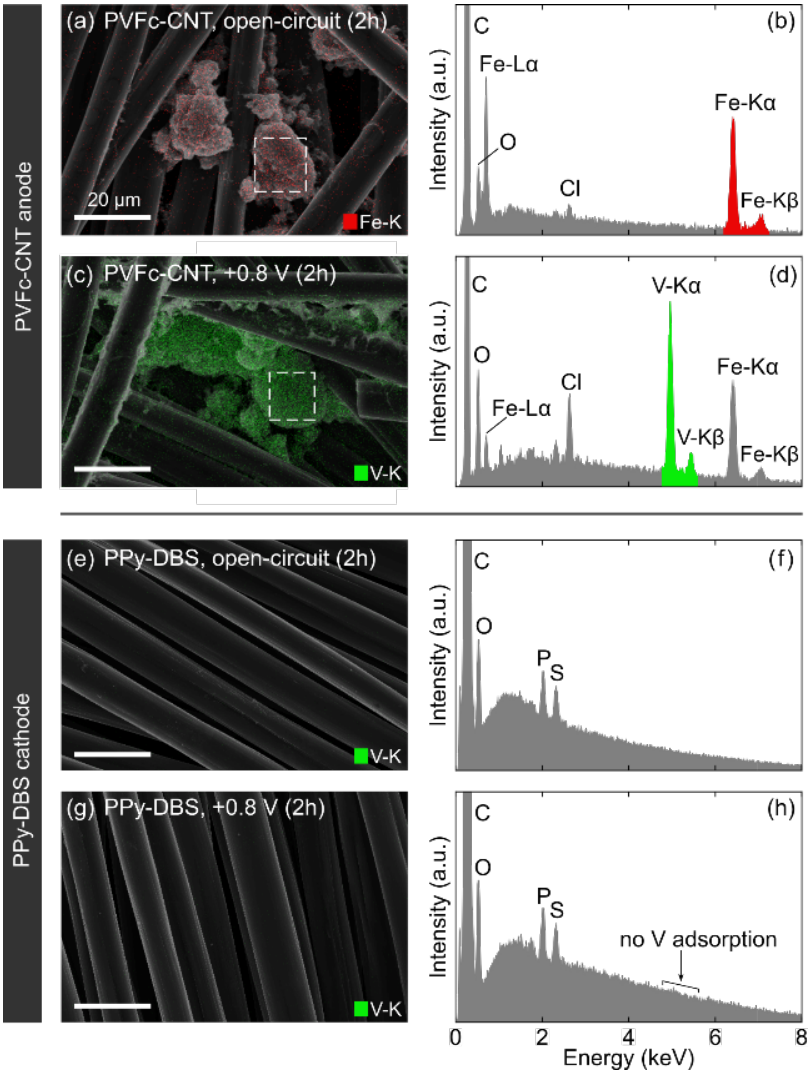

Figure 6. SEM micrographs (left) and EDX spectra (right) of the anode and the cathode at the end of 2 h open circuit and +0.8 V adsorption. Open-circuit operation does not lead to any appreciable vanadium uptake, as evident from the emission spectrum ((a) and (b)). However, charging at +0.8 V results in localized vanadium accumulation into iron-rich PVFc-CNT bundles. Note the presence or lack thereof of vanadium Kα and Kβ emission lines in (b) and (d). On the other hand, as expected, the PPy-DBS electrode does not indicate any vanadium uptake in either case ((e) to (h)).

3.3. Selective vanadium recovery in flow system

In this section, we first discuss selective vanadium recovery in the flow system introduced in **Section 2.4** and later we propose an adsorption/desorption mechanism based on various

analytical methods and detailed observations. Details of experimental conditions are given in **Section 2.4** with an image of the experimental setup in **Figure 2(a)**. The electrodes were 2x12 cm carbon cloth with 0.4 mg cm^{-2} PVFc and 0.75 C cm^{-2} PPy loading, corresponding to about 75 µmoles of PVFc active material. The electrochemical cell was operated potentiostatically (at +1.1 V for charging and -0.5 V for discharging) at a flowrate of 0.48 ml min^{-1} and the effluent solution was sampled frequently for quantification of the anion concentrations. Similar to the batch adsorption detailed in **Section 3.2**, two separate experiments with solutions containing 0.5 mM KVO_3 with and without competing anions were performed.

Figure 7 shows concentration profiles for the three cases measured with IC and ICP-OES. In each experiment, the cell was initially flushed with DI water, and immediately prior to adsorption, the influent was switched to vanadium-containing solution. Experiments reported in **Figures 7(a)** and **7(b)** correspond to 20 mM ClO_4^- with 0.5 mM VO_3^- at 0.48 ml min^{-1} flowrate, while the experiment of **Figure 7(c)** was performed with 20 mM ClO_4^- and 0.1 mM VO_3^- at 0.24 ml min^{-1}. In all cases, the background anion ClO_4^- plateaus at the inlet concentration (20 mM) relatively quickly, while vanadium breakthrough occurs at a slower rate, showing stronger electrochemical interaction of vanadium with the anode surface. Additionally, the breakthrough curves for competing anions in **Figure 7(b)** bear similarities with that of ClO_4^-. The inset of **Figure 7(b)** quantifies adsorbed amounts of individual anions during adsorption and shows around 11 µmoles for vanadium and <1.5 µmoles for other anions, in line with observations in the batch adsorption studies. During desorption at -0.5 V, on the other hand, vanadium and other anions are released from the anode resulting in a rapid concentration increase in the effluent.

The experiment of **Figure 7(c)**, with 5x lower vanadate concentration and 2x slower flowrate, on the other hand, shows a prolonged breakthrough curve with a plateau averaging at ~40% of the inlet vanadate concentration during the adsorption process, demonstrating effective selective capture of vanadium. We hypothesize the none-zero effluent concentration can be attributed to bypassing and/or channeling effects inside the cell, deficiencies that can be overcome with improved cell design and uniform flow distribution.

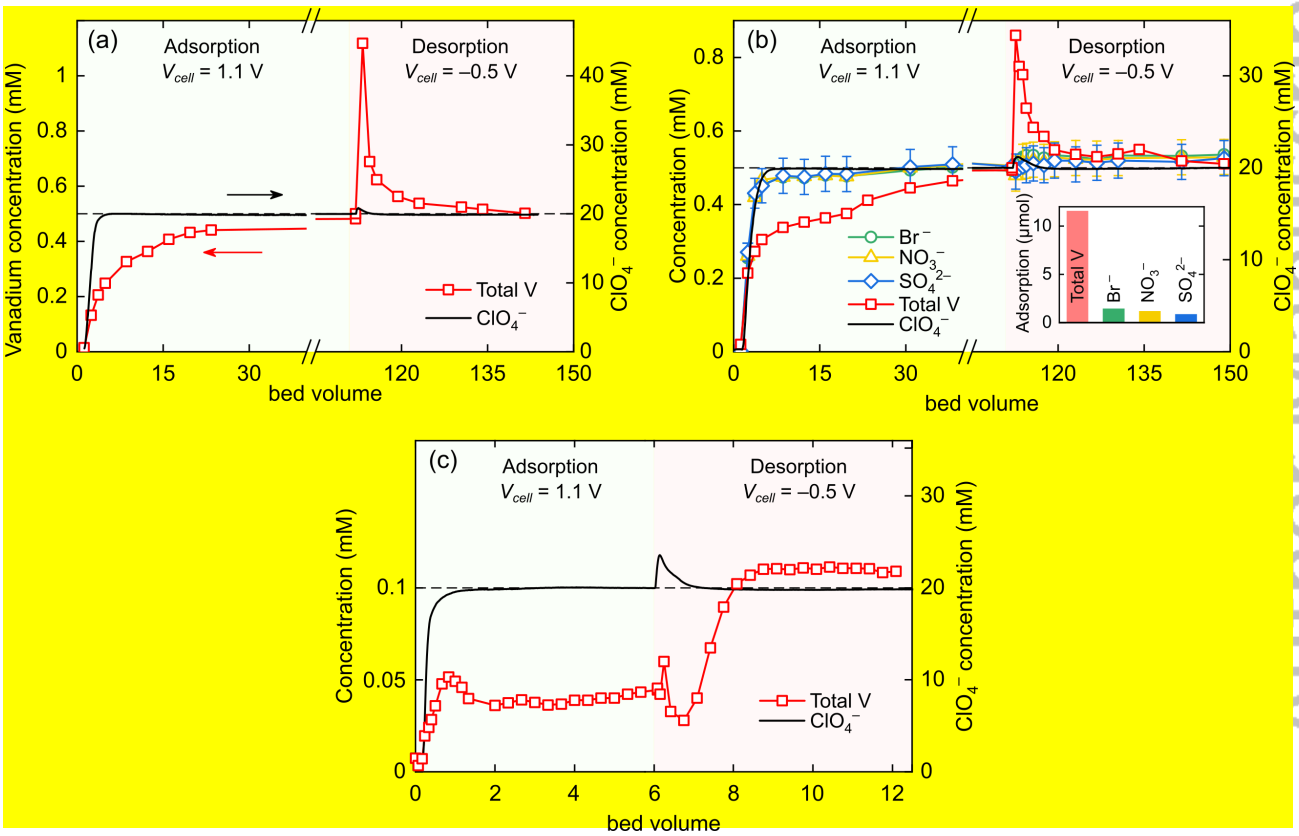

Figure 7. Effluent concentration profiles for vanadium during 1.1 V adsorption and -0.5 V desorption with (a), (b) 0.5 mM VO_3^- at 0.48 ml min^{-1} and (c) 0.1 mM VO_3^- at 0.24 ml min^{-1}. Vanadium breakthrough occurs at a rate slower than that of the background anion or other competing anions, showing stronger affinity of the anode for vanadium oxyanions. Inset of panel (b) quantifies adsorption of individual anions during charging at 1.1 V and confirms strong selectivity towards vanadium. Desorption at -0.5 V results in anions are expulsion from the anode and subsequent rapid concentration increase at the effluent. Panel (c) shows a

prolonged breakthrough curve with more evident plateau during the adsorption step, demonstrating effective and selective vanadium capture compared to the background anion in 200-fold abundance.

Results in **Figure 7(b)** demonstrate selectivity of our flow cell towards vanadium, but do not reveal vanadium speciation during the process or the adsorption/desorption mechanism. Our further analysis to understand such mechanisms suggests the importance of factors such as flowrate and pH environment, as summarized in **Figure 8(a)**. During adsorption, the PPy-DBS electrode sequesters cations including sodium and hydronium and raises the solution pH. As an example, we show in **Figure 8(b)** that the effluent pH (corresponding to the experiment in **Figure 7(b)**) increased to around 9 during adsorption. A portion of the incoming vanadium thus changes from univalent $H_2VO_4^-$ to divalent HVO_4^{2-} and is selectively removed from the solution by the PVFc-CNT electrode. During desorption, on the other hand, pH decreases due to simultaneous sodium and hydronium release from surface of the PPy-DBS electrode, which favors the co-presence of $H_2VO_4^-$ and uncharged H_3VO_4 in the solution. Similarly, **Figure 8(b)** shows an abrupt reduction of effluent pH to around 4 during desorption.

To complement this observation, we monitored the oxidation state of effluent vanadium for possible electrochemical reactions using ultraviolet-visible spectrophotometry (UV-Vis). **Figure S5(a)** of **SI** shows control absorption spectra for V(II) to V(V) and demonstrates distinct absorption peaks in the 400-800 nm range for V(II) through V(IV), but a total absence of an absorption peak for V(V). Results show UV-Vis signals of the adsorption/desorption samples do not contain any appreciable peaks (**Figure S5(b)** of **SI**), which bear similarities to the V(V) control sample and confirm no change in oxidation state of influent V(V) during the adsorption and desorption steps.

Lastly, we note the importance of flowrate and pH management in the performance of our flow device. In general, pH fluctuations are more pronounced under lower flowrates, due to longer residence time and prolonged parasitic reactions. In unfavorable cases with overly slow flowrates where pH decreases below 3, cationic vanadate VO_2^+ can potentially form and subsequently get re-adsorbed electrostatically to the PVFc-CNT electrode. To examine this hypothesis, we performed a separate adsorption study with adsorption (at 1.1 V) similar to that of **Figure 7(a)**, but with the flow stopped for 30 min during the desorption step, followed by a flush step with 0.48 ml min^{-1} flowrate (both at -0.5 V) (see **Figure S6** of **SI**). We hypothesize the 30 min desorption under stopped flow conditions resulted in the formation of cationic VO_2^+ and provided ample time for VO_2^+ re-adsorption. Note that although PVFc moieties are neutral upon reduction, the electrode can still adsorb VO_2^+ into the electric double layers due to negative polarization of the substrate during the discharge step. Effluent vanadium concentration shows an insignificant desorption peak and corroborates the vanadate re-adsorption supposition (**Figure S6** of **SI**). Moreover, the EDX elemental map and spectrum of PVFc-CNT after desorption show noticeable amounts of re-adsorbed vanadium on the surface (**Figure S7** of **SI**). We note that vanadium distribution in this case is mostly uniform across the surface and not localized to iron-rich CNT bundles, further verifying electrostatic and non-selective re-adsorption. Additionally, as expected, the PPy-DBS surface does not show any noticeable vanadium uptake.

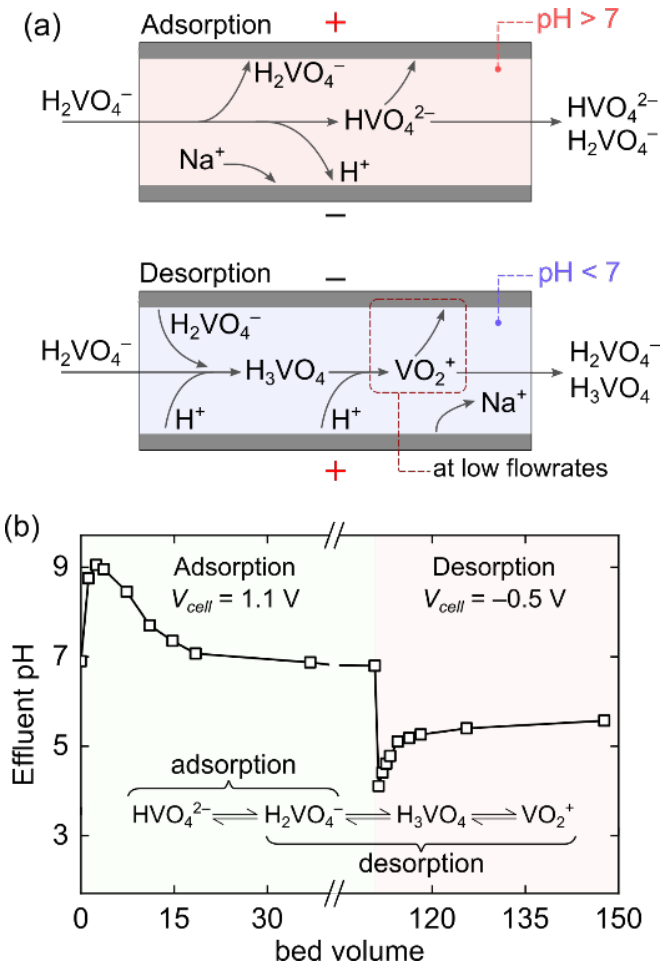

Figure 8. (a) The proposed vanadium speciation and adsorption/desorption mechanism. Uptake of sodium and hydronium during adsorption increases the local pH and favors formation of HVO_4^{2-}. The co-existing $H_2VO_3^-$ and HVO_4^{2-} are then selectively removed by PVFc-CNT. During desorption, pH decreases and favors formation of $H_2VO_3^-$ and H_3VO_4. In cases with excessively low flowrate and low pH (pH<3), anionic VO_2^+ can form and subsequently get re-adsorbed onto the PVFc-CNT electrode. (b) Effluent pH corresponding to **Figure 7(a)**. pH during adsorption rises to around 9, favoring formation of univalent and divalent vanadate, while pH during desorption decreases to around 4, favoring univalent and uncharged vanadate. In unfavorable cases with pH < 3, cationic vanadate can form and subsequently, re-adsorb to the PVFc-CNT electrode.

Conclusions

The selective removal and recovery from polluted aqueous streams of heavy metals used in a multitude of industries is of great importance if their environmental impact is to be mitigated successfully. A scalable and efficient platform based on an asymmetric electrochemical cell with continuous flow has been shown to be effective in the selective recovery of vanadium(V) oxyanions from aqueous streams. The system employed the intrinsic affinity for oxyanion species of the redox-active metallocene polymer PVFc on the anode, which was paired with a matched-capacity cathode featuring conductive polymer PPy doped with DBS. The respectable selectivity of >10 relative to the background anion present in a 40-fold abundance, and in the presence of various competing anions, attests to the promise for such electrochemically mediated separations to address environmental contamination problems, as well as for resource recovery from process and recycle streams. The advantage of the electrochemical modulation of ion-exchange capacity and selectivity over traditional technologies is that it can be based entirely on simple voltage swings, and it does not require the use of chemical agents to release the ions once they are captured, therefore eliminating the secondary waste problems associated with other separation approaches.

Moving forward, the redox-active electrode moieties can potentially be modified chemically to provide enhanced selectivity toward desired species, not only toward oxyanions, but also toward a wide range of other anionic and cationic compounds. Additionally, the successful implementation of the platform technology demonstrated here will require that the chemical and physical stability of the electrodes be maintained over many adsorption/desorption cycles, with high active material loading and electrode area to achieve higher capacity suitable for industrial applications, as well as effective engineering to minimize performance degradation due to poor flow patterns, which can lead to bypassing, channeling

and backmixing within the flow channel. In short, electrochemically based separations technologies provide a versatile approach to tackle many industrial and environmental problems in an era in which the future electrification of our industries is becoming more and more evident.

Acknowledgements

N.O. greatly appreciates the support by The Scientific and Technological Research Council of Turkey (TÜBİTAK), 2219 International Postdoctoral Research Scholarship Program. This work made use of the MRSEC Shared Experimental Facilities at MIT.

Supporting Information

The Supporting Information presents details of anions quantification and supplementary measurements of adsorption kinetics, current, and effluent pH, as well as complementary UV-Vis and X-ray microanalysis.

References

[1] M. Omidinasab, N. Rahbar, M. Ahmadi, B. Kakavandi, F. Ghanbari, G. Z. Kyzas, S. S. Martinez, N. Jaafarzadeh, *Environ. Sci. Pollut. Res.* **2018**, *25*, 34262–34276.
[2] S. Jana, J. Ray, D. Jana, B. Mondal, S. K. Bhanja, T. Tripathy, *Colloids Surfaces A Physicochem. Eng. Asp.* **2019**, *566*, 70–83.
[3] J. H. Huang, F. Huang, L. Evans, S. Glasauer, *Chem. Geol.* **2015**, *417*, 68–89.
[4] J. P. Gustafsson, *Appl. Geochemistry* **2019**, *102*, 1–25.
[5] H. I. Gomes, A. Jones, M. Rogerson, G. M. Greenway, D. F. Lisbona, I. T. Burke, W. M. Mayes, *J. Environ. Manage.* **2017**, *187*, 384–392.
[6] Q. He, S. Si, J. Zhao, H. Yan, B. Sun, Q. Cai, Y. Yu, *Saudi J. Biol. Sci.* **2018**, *25*, 1664–1669.
[7] IARC (International Agency for Research on Cancer), *IARC Monogr. Eval. Carcinog. risks to humans* **2006**, *86*, 1–294.
[8] M. Buchman, *Screening Quick Reference Tables (SQuiRTs)*, **2008**.
[9] X. Xu, B. Gao, B. Jin, Q. Yue, *J. Mol. Liq.* **2016**, DOI 10.1016/j.molliq.2015.12.101.

[10] P. Roccaro, F. G. A. Vagliasindi, *Desalin. Water Treat.* **2015**, *55*, 799–809.
[11] R. M. M. Riofano, L. C. Casteletti, L. C. F. Canale, G. E. Totten, *Wear* **2008**, *265*, 57–64.
[12] K. Nomura, S. Zhang, *Chem. Rev.* **2011**, *111*, 2342–2362.
[13] C. Ding, H. Zhang, X. Li, T. Liu, F. Xing, *J. Phys. Chem. Lett.* **2013**, *4*, 1281–1294.
[14] K.-L. Yang, T.-Y. Ying, S. Yiacoumi, C. Tsouris, E. S. Vittoratos, *Langmuir* **2001**, *17*, 1961–1969.
[15] A. Naeem, P. Westerhoff, S. Mustafa, *Water Res.* **2007**, *41*, 1596–1602.
[16] A. Keränen, T. Leiviskä, A. Salakka, J. Tanskanen, *Desalin. Water Treat.* **2015**, *53*, 2645–2654.
[17] T. Leiviskä, M. K. Khalid, A. Sarpola, J. Tanskanen, *J. Environ. Manage.* **2017**, *190*, 231–242.
[18] L. Luo, T. Miyazaki, A. Shibayama, W. Yen, T. Fujita, *Miner. Eng.* **2003**, *16*, 665–670.
[19] L. Luo, L. Kejun, A. Shibayama, W. Yen, T. Fujita, O. Shindo, A. Katai, *Hydrometallurgy* **2004**, *72*, 1–8.
[20] T. Leiviskä, A. Keränen, N. Vainionpää, J. Al Amir, O. Hormi, J. Tanskanen, *Water Sci. Technol.* **2015**, *72*, 437–442.
[21] H. Sharififard, M. Soleimani, *RSC Adv.* **2015**, *5*, 80650–80660.
[22] T. R. S. Cadaval, G. L. Dotto, E. R. Seus, N. Mirlean, L. A. de Almeida Pinto, *Desalin. Water Treat.* **2016**, *57*, 16583–16591.
[23] Y. Yu, M. Liu, J. Yang, *Chem. Ecol.* **2018**, *34*, 548–564.
[24] Q. He, S. Si, J. Zhao, H. Yan, B. Sun, Q. Cai, Y. Yu, *Saudi J. Biol. Sci.* **2018**, *25*, 1664–1669.
[25] A. Naeem, P. Westerhoff, S. Mustafa, *Water Res.* **2007**, *41*, 1596–1602.
[26] X. ZHU, G. HUO, J. NI, Q. SONG, *Trans. Nonferrous Met. Soc. China* **2017**, *27*, 2727–2732.
[27] J. Duan, S. Bao, Y. Zhang, *Chem. Eng. Res. Des.* **2018**, *132*, 178–186.
[28] L. Wang, G. Zhang, W. Guan, L. Zeng, Q. Zhou, Y. Xia, Q. Wang, Q. Li, Z. Cao, *Hydrometallurgy* **2018**, *179*, 268–273.
[29] S. K. Tangri, A. K. Suri, C. K. Gupta, *Trans. Indian Inst. Met.* **1998**, *51*, 27–39.
[30] L. Luo, T. Miyazaki, A. Shibayama, W. Yen, T. Fujita, *Miner. Eng.* **2003**, *16*, 665–670.
[31] S. Akita, T. Maeda, H. Takeuchi, *J. Chem. Technol. Biotechnol.* **1995**, *62*, 345–350.
[32] K. L. Yang, T. Y. Ying, S. Yiacoumi, C. Tsouris, E. S. Vittoratos, *Langmuir* **2001**, *17*, 1961–1969.
[33] X. Su, H. J. Kulik, T. F. Jamison, T. A. Hatton, *Adv. Funct. Mater.* **2016**, *26*, 3394–3404.
[34] X. Su, T. A. Hatton, *Adv. Colloid Interface Sci.* **2017**, *244*, 6–20.
[35] K. Tan, X. Su, T. A. Hatton, *Adv. Funct. Mater.* **2020**, *30*, 1910363.
[36] D. I. Oyarzun, A. Hemmatifar, J. W. Palko, M. Stadermann, J. G. Santiago, *Water Res. X* **2018**, *1*, 100008.
[37] D. I. Oyarzun, A. Hemmatifar, J. W. Palko, M. Stadermann, J. G. Santiago, *Sep. Purif. Technol.* **2018**, *194*, 410–415.
[38] X. Su, A. Kushima, C. Halliday, J. Zhou, J. Li, T. A. Hatton, *Nat. Commun.* **2018**, *9*, 4701.
[39] A. Brennsteiner, J. W. Zondlo, A. H. Stiller, P. G. Stansberry, D. Tian, Y. Xu, *Energy and Fuels* **1997**, *11*, 348–353.
[40] R. Chen, T. Sheehan, J. L. Ng, M. Brucks, X. Su, *Environ. Sci. Water Res. Technol.* **2020**, DOI 10.1039/c9ew00945k.
[41] X. Mao, G. C. Rutledge, T. A. Hatton, *Langmuir* **2013**, *29*, 9626–9634.
[42] Y. Ren, Z. Lin, X. Mao, W. Tian, T. Van Voorhis, T. A. Hatton, *Adv. Funct. Mater.* **2018**, *28*, 1–12.

[43] M.-A. De Paoli, R. C. D. Peres, S. Panero, B. Scrosati, *Electrochim. Acta* **1992**, *37*, 1173–1182.
[44] M. A. Careem, Y. Velmurugu, S. Skaarup, K. West, *J. Power Sources* **2006**, *159*, 210–214.
[45] T. Matencio, M.-A. De Paoli, R. C. D. Peres, R. Torresi, S. I. C. de Torresi, *J. Braz. Chem. Soc.* **1994**, *5*, 191–196.
[46] Y. Ren, X. Mao, T. A. Hatton, *ACS Cent. Sci.* **2019**, *5*, 1396–1406.
[47] C. Zhao, W. Zheng, *Front. Energy Res.* **2015**, *3*, 1–11.

609 **TOC**
610

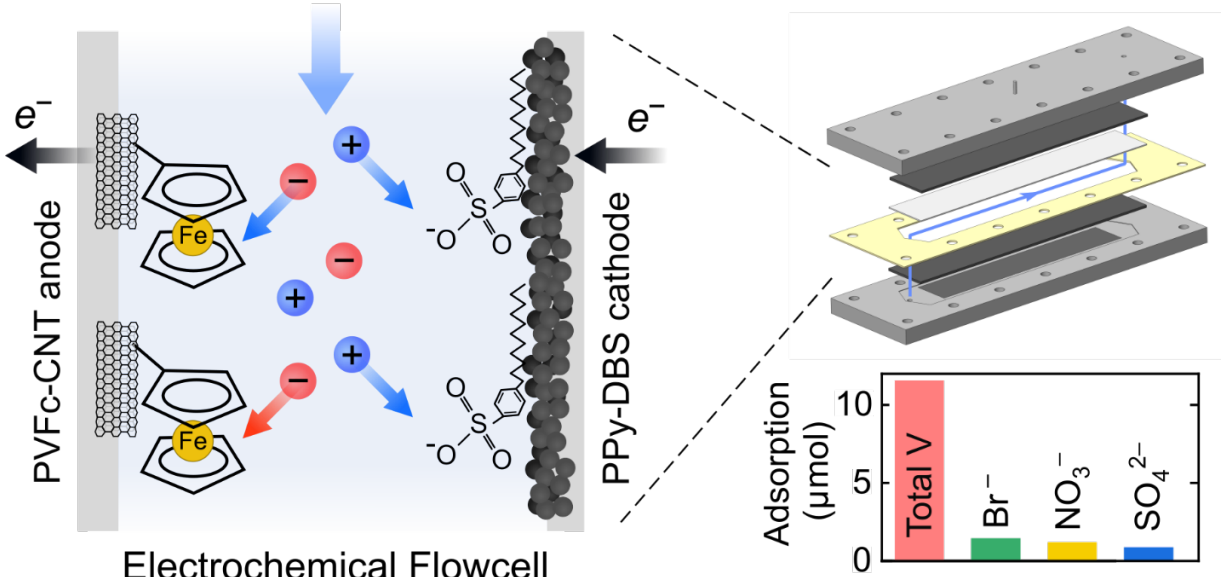

611
612

613 An asymmetric, redox-active electrochemical flow platform for selective recovery of
614 vanadium(V) oxyanions from aqueous streams with demonstrated selectivity of >10 against
615 the background anion with 40-fold in abundance.